**TABLE OF CONTENTS (TOC)**

**Silicene on non-metallic substrates: recent theoretical and experimental advances**

E. Scalise[1](□), K. Iordanidou[2], V.V. Afanas'ev[2], A. Stesmans[2] and M. Houssa[2] (□)

[1]Max-Planck-Institut für Eisenforschung, Germany

[2]University of Leuven, Belgium.

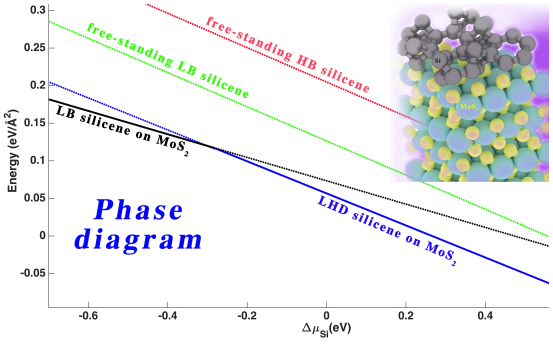


A review of recent theoretical and experimental works on the possible growth of silicene on non-metallic surfaces.

A theoretical approach to systematically study the stability of silicene on substrates.

*Nano Research*
DOI (automatically inserted by the publisher)
Review Article

ISSN 1998-0124
CN 11-5974/O4

# Silicene on non-metallic substrates: recent theoretical and experimental advances

E. Scalise[1](✉), K. Iordanidou[2], V.V. Afanas'ev[2], A. Stesmans[2] and M. Houssa[2] (✉)

[1]*Max-Planck-Institut für Eisenforschung, Max-Planck Straße 1, D-40237 Düsseldorf, Germany*
[2] *Department of Physics and Astronomy, University of Leuven, Celestijnenlaan 200D, B-3001 Leuven, Belgium.*

**Received:** day month year
**Revised:** day month year
**Accepted:** day month year (automatically inserted by the publisher)



## KEYWORDS

silicene, non-metallic substrates, chalcogenide, $MoS_2$, layered compounds.

## ABSTRACT

Silicene, the silicon counterpart of graphene, has so far been successfully grown on metallic substrates, like Ag(111), $ZrB_2$(0001) and Ir(111) surfaces. However, the characterization of its electronic structure is hampered by the metallic substrate. In addition, potential applications of silicene in nanoelectronic devices will require its growth/integration with semiconducting or insulating substrates. We revisit recent theoretical works about the interaction of silicene with several non-metallic templates, distinguishing between the weak van der Waals like interaction of silicene with e.g. layered metal (di)chalcogenides, and the stronger covalent bonding between silicene and e.g. ZnS surfaces. We then present a methodology to effectively compare the stability of diverse silicene structures for different synthesis conditions, by exploiting thermodynamics and molecular dynamics density functional theory calculations. Recent experimental results on the possible growth of silicene on $MoS_2$ are also highlighted and compared to the theoretical predictions.

TSINGHUA UNIVERSITY PRESS Springer

## 1.Introduction

Since the isolation and characterization of graphene in 2004 [1,2], two-dimensional materials are triggering an enormous interest, both fundamentally and technologically [3-5]. Recently, the possible growth of single atomic layers of the other group-IVa elements (Si, Ge and Sn) has emerged [6-9]. Silicene, for example, is the Si counterpart of graphene, i.e. a single layer of Si atoms arranged in a hexagonal network. This novel 2D material has been extensively studied theoretically [10-16], as well as experimentally [17-24]. Indeed, the synthesis of silicene on various metallic substrates, like (111)Ag surfaces [6,17-21], (0001)$ZrB_2$ surfaces [22,23] and (111)Ir [24] surfaces, has been reported. A recent breakthrough paved the way to the possible realization of silicene-based field effect transistors operating at room temperature [25], presenting ambipolar current-voltage characteristics, as expected for a gapless semiconductor.

A clear advantage of silicene, over graphene, for nanoelectronic devices is its compatibility with the existing silicon-based nanotechnology. Another advantage of silicene lies in its atomic structure: free-standing silicene is predicted to be buckled, with a buckling distance of about 0.44 Å [11]. The buckling arises from the mixed $sp^2$-$sp^3$ character of Si atoms, and it is predicted to be a key feature for the possible functionalization of its electronic properties [26-29], as will also be highlighted below.

So far, experimental evidences for the growth of silicene has been obtained on metallic substrates. However, the characterization of the electronic and electrical properties of silicene on metallic substrates is very challenging, since these properties are then largely dominated by the metal. The growth of silicene on semiconducting or insulating substrates is required for their firm identification and complete characterization. In addition, potential applications of this novel 2D material in nanoelectronic devices will also require its growth and integration on non-metallic substrates.

We revisit here recent theoretical results, essentially based on density-functional theory calculations, pertaining to the interaction of silicene with non-metallic surfaces (mostly from ref. [30, 35, 54, 65]). We first discuss the weak (van der Waals) interaction of silicene with e.g. AlN and layered dichalcogenide substrates. On these templates, silicene was predicted to be either metallic, semi-metallic (with preserved Dirac cones at the k-points), or semiconducting, depending on its buckling and degree of interaction with the substrate. We also show results on the stability of diverse silicene structures, including the so-called dumbbell silicene structure, on layered dichalcogenide substrates. These results were obtained based on a thermodynamic approach and confirmed by molecular dynamics (MD) simulations. We highlight the efficiency of this approach to systematically investigate the stability of so-called van der Waals heterostucture such as the weak interacting silicene/layered dichalcogenide systems. Recent experimental results on the possible growth of silicene on $MoS_2$ [35] are discussed and compared to the theoretical predictions. The fabrication of transistors incorporating Si/$MoS_2$ heterosheet [58], functioning at room temperature, is also highlighted.

We next discuss the covalent bonding of silicene on e.g. (0001)ZnS surfaces. The charge transfer occurring at the silicene/(0001) ZnS interface leads to the opening of an indirect energy band gap in silicene. Very interestingly, it was found that the nature (indirect or direct) and magnitude of its energy band gap could be controlled by an external electric field. Analogous modulation of the bandgap, induced by charge reorganization at the silicene interface, was recently reported for weak interacting silicene/ $SnS_2$ heterostucture [75], confirming a result potentially very interesting for field-effect devices.

## 2. Silicene/substrate interaction: weak van der Waals bonding

Layered semiconducting materials, with strong intra-layer covalent bonding and weak inter-layer van der Waals bonding, are expected to interact weakly with silicene, potentially preserving its peculiar electronic properties [30-38]. We discuss here the weak interaction of silicene with two different type of layered materials, namely graphite-like AlN [30,31] and semiconducting

Address correspondence to E.Scalise, scalise@mpie.de; M. Houssa, michel.houssa@kuleuven.be

(transition) metal dichalcogenides [32-35, 75].

AlN is an insulator (energy band gap of about 6.5 eV [39]) which crystallizes in the wurtzite phase, with in-plane lattice parameters a=b=3.11 Å and out-of-plane lattice parameter c=4.98 Å [40]. Very interestingly, the polar (0001) AlN surface is predicted to evolve to a more stable graphite-like structure [30,41], with the Al and N atoms adopting a $sp^2$-hydridization. The graphite-like form of AlN is insulating, with a computed energy band-gap of about 4.6 eV, and is more stable than the (0001) AlN polar surface by about 0.27 eV/atom [30]. This predicted structural and electronic ''phase transition'' in AlN is consistent with first-principles calculations on ultra-thin wurtzite films [41]. The driving force for the planarization and $sp^2$-hybridization of the AlN layers is the suppression of the strong dipole between the bottom and the top surface of the film, which are terminated either by anions or cations; this transition depends on the electronegativity difference between the anions and cations as well as the energy gap of the material, leading to a thickness dependence of this transition [41]. The graphite-like form of AlN is predicted to be more stable than the (0001) wurtzite structure up to 24 layers, corresponding to a layer thickness of about 2.6 nm. Very interestingly, the possible growth of graphite-like AlN on Ag (111) surfaces has been recently observed experimentally [42].

The possibility of inserting a silicene "flake" (i.e. a silicene ribbon terminated by H atoms) in-between a graphite-like AlN lattice was then considered [30,31]. In this configuration, the top AlN layer could serve as an efficient barrier against the diffusion of chemical species towards the silicene surface. The starting configuration corresponds to a compressively strained flat silicene ribbon inserted between two AlN layers, as shown in Fig. 1. The studies [30,31] found that during the energy relaxation, the Si-Si bond length increases and reaches its free-standing value of about 2.2 Å. After relaxation, the silicene layer is buckled, with a buckling distance of about 0.21 Å, which is lower than its predicted free-standing buckling distance

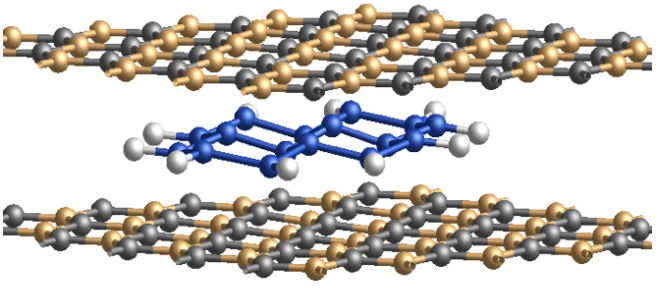

**Figure 1** Relaxed atomic configuration of a AlN/silicene/AlN (van der Waals) heterostructure. Dark gray, light orange, blue and white spheres represent Al, N, Si and H atoms, respectively. Reproduced with kind permission from AIP Publishing, ref. [30].

(about 0.44 Å). In this configuration, the silicene layer weakly interacts with the AlN layers via van der Waals forces, the computation of the partial (Mulliken) atomic charges on the Si, Al, and N atoms indicating no net charge transfer between Si and the Al or N atoms. However, the weak interaction between the Si $p_z$ orbitals and the out-of-plane dipole formed between the Al and N atoms from the bottom and top AlN layers, respectively, is likely responsible for the reduced silicene buckling, as compared to its

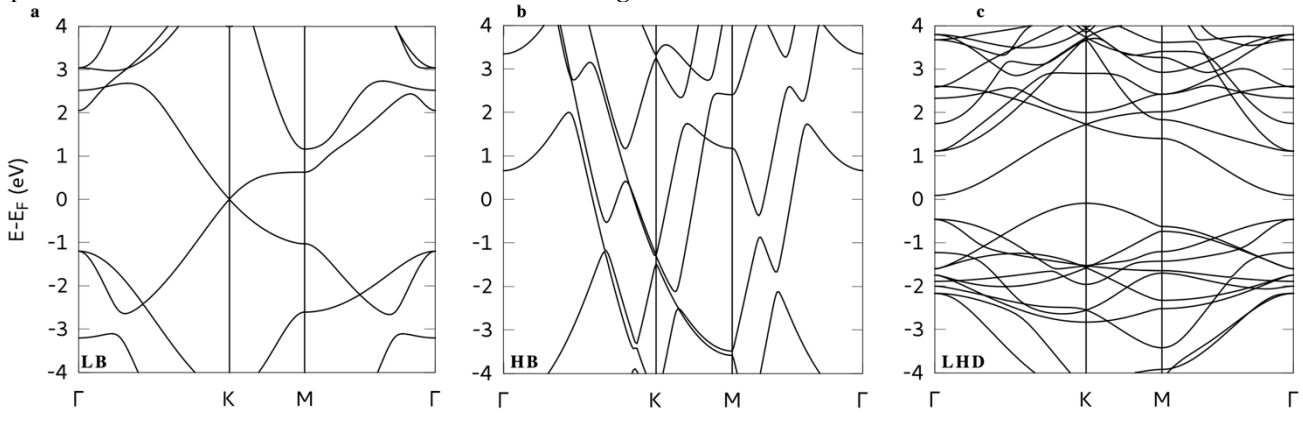


**Figure 2** Electronic band structure of free-standing low buckled (LB) silicene (a), high buckled (HB) silicene (b), large honeycomb dumbbell (LHD) silicene (c).

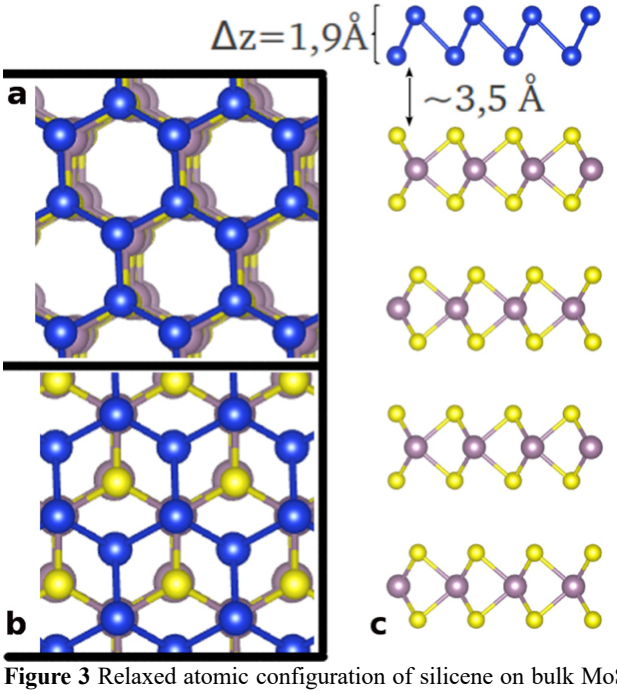


**Figure 3** Relaxed atomic configuration of silicene on bulk $MoS_2$ (in a and c the top and side view is shown, respectively). In (b) the top view of a different configuration is also shown. Blue, yellow and purple spheres are Si, S and Mo atoms, respectively. Reproduced with kind permission from IOP Publishing, ref. [35].

free-standing configuration. In this van der Waals like AlN/silicene/AlN heterostructure, silicene is predicted to be a gapless semiconductor (see Fig. 2a), due to the preserved $sp^2$-$sp^3$ mixed hybridization of the Si atoms, thus preserving the linear dispersion behavior, typical for low buckled (LB) free standing silicene [11].

Van der Waals interactions play also a crucial role for the family of materials known as (layered) transition metal chalcogenides, having $MoS_2$ as the most noted representative. These materials are composed by metal-chalcogenide layers, having a hexagonal structure similar to silicene, which are kept together by the van der Waals interactions. Ionic-covalent bonds between the transition metal and the chalcogenide elements ensure the in-plane stability of the layers. Because of their layered structure, transition metal chalcogenide bulk crystals can be exfoliated in order to obtain few-layers thin flakes or even monolayers, with "ideal" surfaces having no dangling bonds. Thus, transition metal chalcogenides are perfect substrates for other (2D) layered materials, such as graphene, and optimal candidate as template for silicene.

$MoS_2$ is an indirect band-gap semiconductor (gap=1.2 eV [43]) and its hexagonal structure has an in-plane lattice parameter of 3.16 Å [43] (about 18.3% smaller than the lattice parameter of free standing silicene). Single layer $MoS_2$ is a direct-gap semiconductor with a band-gap of about 1.9 eV [44-46]. Suspended mono-layer $MoS_2$ has also been realized [47,48] and its properties have been investigated both experimentally [44-46] and theoretically [49-51].

The interaction of silicene with $MoS_2$ was first investigated in ref. [35], by modeling a flat hexagonal Si layer on the $MoS_2$ surface. Note that in this study the lattice parameter of the heterostructure was fixed to the $MoS_2$ one (3.16 Å), thus considering the case of a fully strained silicene layer on $MoS_2$. Different possible arrangements of the Si atoms, with respect to the underlying Mo and S atoms were also considered, as discussed in more details in ref. 35. Results showed that after energy relaxation, the silicene layer placed on $MoS_2$ is highly buckled, with a vertical distance between the Si top and bottom atoms of about 1.9 Å (cf. Fig. 3).

The energy difference between the various arrangements of silicene on $MoS_2$ is predicted to be about 3 meV/atom, indicating a degeneracy of the different configurations and hence very weak (van der Waals) interactions between silicene and $MoS_2$. The adhesion energy of the silicene layer on $MoS_2$, estimated as the difference between the energy of the silicene/$MoS_2$ system and the sum of the energies of the isolated silicene layer and $MoS_2$ substrate, was calculated to be about 200 meV per unit cell. This is a value very close to the reported interlayer binding energy in bulk-layered materials, like graphite [52], thus confirming the vdW nature of the Si/$MoS_2$ interaction. The Si/$MoS_2$ interlayer distance was calculated to be about 3.5 Å (cf. Fig. 3), a value comparable to the typical inter-layer distance in vdW-bonded layered materials, like $MoS_2$, h-BN or graphite [52].

Both the Si buckling distance and the Si-$MoS_2$ distances obtained from these DFT simulations were in very good agreement with experimental STM results (see Fig. 4), where the step profile between a Si domain and the $MoS_2$ substrate amounts to 3 Å and exhibits a feature at about 2Å consistently with

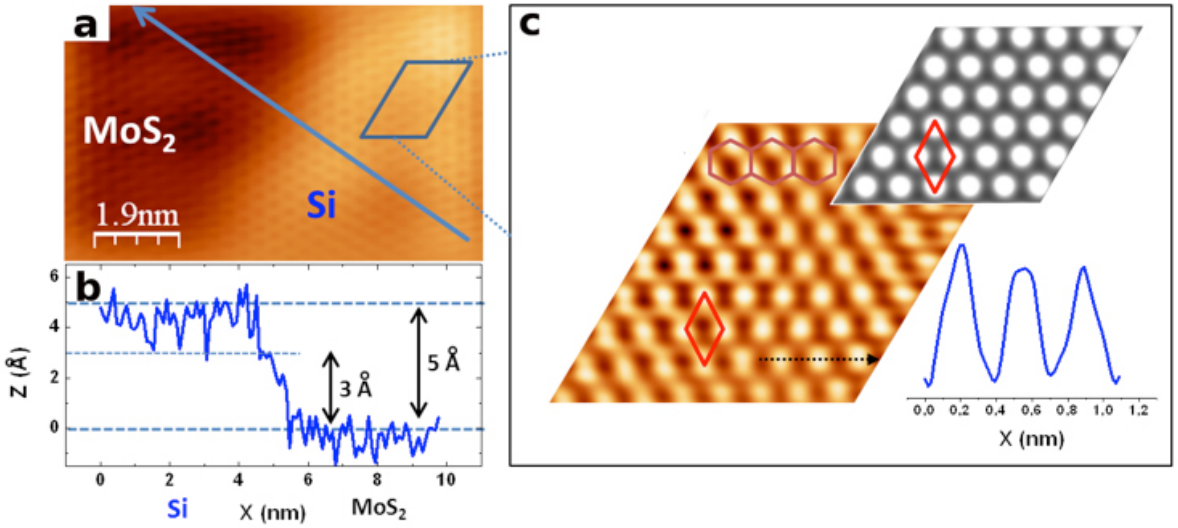


**Figure 4** (a) High resolution STM image of a partially Si-covered $MoS_2$ surface. The left side and the right side of the image corresponds to a portion of bare $MoS_2$ and a Si covered region, respectively. A line profile taken across the two terraces, measuring the amplitude of the step, is shown in (b). In (c) the magnified topography after (fast Fourier transform) filtering evidences the hexagonal surface. A simulated STM image of silicene on $MoS_2$ is shown as (top) inset. A line profile following the black arrow drawn in the STM image is plotted in the bottom inset. Reproduced with kind permission from IOP Publishing, ref. [35].

the highly buckled silicene arrangement (Fig. 3.c). Details about the experiments can be found in ref. [34]. The simulated highly buckled (HB) freestanding silicene structure [11] was predicted to be metallic (cf. Fig.2b), contrary to the low buckled and flat layers. The calculated band structure and local density of states (LDOS) for silicene on bulk $MoS_2$ also indicated a metallic character [35]. Particularly, the LDOS showed that the density of states of the $MoS_2$ substrate still preserves a gap very close to that of the bare $MoS_2$, while all the electronic states close to the Fermi level are due to the contribution of Si atoms, confirming that almost no hybridization between Si and Mo/S atomic orbitals is induced.

The theoretical results obtained on HB silicene/$MoS_2$ heterostructures can be compared with DFT simulations performed on low strained, low buckled silicene on $MoS_2$ [53,54]. In this case, larger supercells were used, in order to minimize the lattice mismatch between silicene and $MoS_2$, as illustrated in Fig. 5 (a). After relaxation, the silicene layer is predicted to be low buckled, with a typical buckling distance of about 0.5 Å (very close to free-standing silicene) and the computed silicene/$MoS_2$ interlayer distance is about 3 Å. The weak van der Waals interaction between LB silicene and $MoS_2$ leads to the opening of a small energy gap in the silicene electronic structure, with preserved Dirac cones [53,54], as shown in Fig. 5 (b). The opening of this energy gap near the Fermi level results from the stronger interaction between the $MoS_2$ substrate and the bottom Si atoms forming an intrinsic interface dipole, which breaks the symmetry between the two sublattices in silicene.

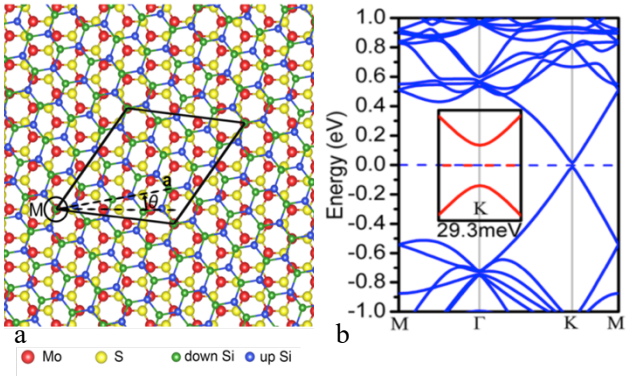


**Figure 5** Atomic configuration (a) and corresponding energy band structure (b) of low buckled silicene on $MoS_2$. The inset in (b) shows a zoom-in of the energy bands near the K point. Reproduced with kind permission from ACS Publishing, ref. [54].

The energy gap of LB silicene on $MoS_2$ can be further controlled by an out-of-plane electric field [53,54]. This electric field induces a redistribution of electrons between the top and bottom Si atoms, and leads to a linear dependence of the energy gap with the electric field. Depending on the direction of this electric field,

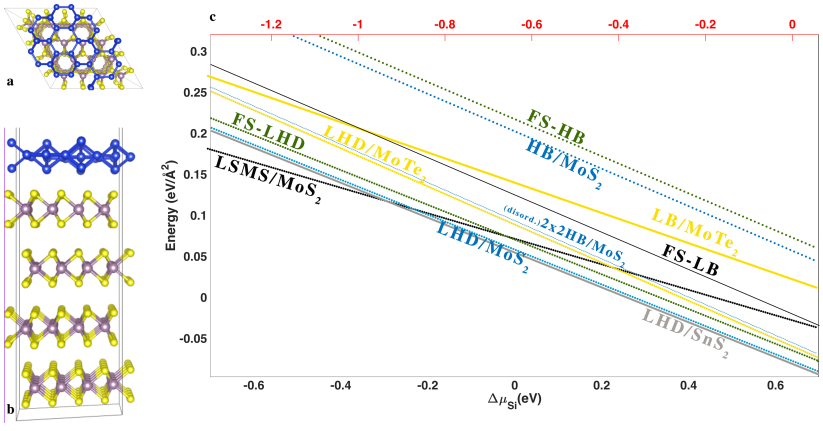


**Figure 6** Top (a) and side (b) view of LHD silicene on $MoS_2$. (c) Phase diagram of silicene on $MoS_2$, $MoTe_2$ and $SnS_2$ substrates. The surface formation energy is plotted as function of the deviation ΔμSi from the reference chemical potential, which is diamond bulk silicon (bottom axis) or LB free standing silicene (top axis), as described in the text. LB and HB indicate the low buckled or high buckled silicene phases. LSMS and LDHS are the low buckled low strained silicene on $MoS_2$ (ref. [35]) and large honeycomb silicene phase [75], respectively. FS indicate the freestanding silicene layer.

the energy gap can be either increased, or decreased [54]. This effect is potentially much interesting for the application of silicene in field effect transistors.

Although further experimental investigations are necessary to corroborate the growth of silicene on $MoS_2$, the comparison of the experimental measurements on Si nanosheets with local hexagonal symmetry [34] and the computed structural and electronic properties of HB and LB silicene on $MoS_2$ clearly confirms the former as the most plausible structure for the first Si nanosheets synthetized on $MoS_2$. However, this cannot be explained by the DFT total energy calculations, which indicate the LB silicene to be more stable than the HB structures on $MoS_2$ by about 350 meV per Si atoms. Thus, we present a comprehensive study of the stability of silicene on $MoS_2$, by employing a grand-canonical thermodynamic approach, analogously to a recent study of silicene on layered $SnS_2$ [75]. This approach is very efficient to probe the stability of the different silicene structures on layered materials, at specific experimental conditions (i.e. chemical potentials), thus mimicking the growth conditions.

In Fig.6 we plot the derived phase diagram versus the variation ($\Delta\mu_{Si} = \mu_{Si} - \mu_{Si,ref}$) of the chemical potential of the silicon reservoir ($\mu_{Si}$) with respect to a reference chemical potential ($\mu_{Si,ref}$). $\mu_{Si,ref}$ was chosen equal to the chemical potential of a reservoir of ideal freestanding silicene [$\mu_{Si,ref}=\mu_{Si}$(silicene)]; or set to the bulk silicon value [$\mu_{Si,ref}=\mu_{Si}$(bulk)]. In fact, $\mu_{Si}$(bulk)] corresponds the limit value for the Si chemical potential, beyond which the appearance of $sp^3$ hybridized Si occurs. The formation free energy γ was then calculated as:

$$\gamma = \frac{1}{A}\left[E_{slab}(n_{Si}, n_{ME_2}) - n_{Si}\Delta\mu_{Si} - n_{Si}\mu_{Si,ref} + -n_{ME_2}\mu_{ME_2}(bulk)\right],$$

with A the surface area of the slab. $n_{Si}$ are the number of Si atoms of the silicene layer and $n_{ME_2}$ are the $ME_2$ units of the layered dichalcogenide, e.g. $MoS_2$ (M for the metal atom and E for the chalcogen). $\mu_{ME2}$(bulk) indicates the chemical potential of the bulk dichalcogenide.

We also include in the calculations of the phase diagram of silicene on layered chalcogenides a different silicene phase, not discussed above, the so-called large honeycomb dumbbell (LHD) silicene. This particular silicene structure is made up of "dumbbell" units of Si atoms in honeycomb arrangement and have been recently simulated on layered $SnS_2$ [75], resulting in the most thermodynamically stable silicene phase on that substrate. Because of its dumbbell structure, shown in the inset of Fig. 7, the Si atoms laying on the central plane of the LHD silicene are 4-fold

coordinated, thus conferring an $sp^3$-like character to this silicene phase. The band structure shown in Fig. 2c shows that free-standing LHD silicene is predicted to be semiconducting, with a gap of about 0.19 eV. The lattice parameter of a free standing LHD silicene was calculated to be 7.38 Å, and a √3×√3 LHD silicene supercell can be built (see Fig. 7), with a corresponding lattice parameter of about 12.78 Å. Thus, the √3×√3 LHD silicene matches very well a 4x4 $MoS_2$ supercell, minimizing the strain of the resulting silicene layer on $MoS_2$ (see Fig. 6 a and b).

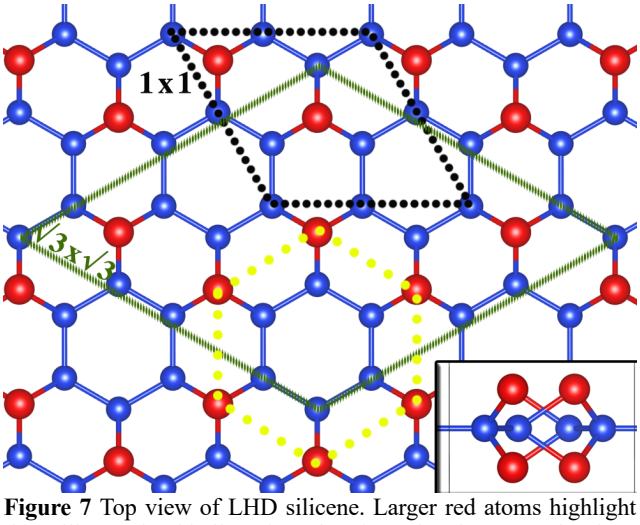


**Figure 7** Top view of LHD silicene. Larger red atoms highlight the silicon dumbbell units, forming the honeycomb rings evidenced by the yellow line. Black and green lines define the 1x1 and √3×√3 cells of LHD silicene, respectively. The inset shows a side view of the LHD unit cell.

From the phase diagram in Fig. 6c, one can assert that LHD silicene is the most stable silicene phase on $MoS_2$ as well, for a broad range of the Si chemical potential. In fact, the surface formation energy of LHD silicene on $MoS_2$ is very close to that of LHD silicene on $SnS_2$, with a difference of only few meV/Å. However, in Si-poor conditions ($\Delta\mu Si$<-0.28 eV, with $\mu_{Si}$(bulk) as reference chemical potential), the formation of low buckled and low strained silicene on $MoS_2$ (LSMS) becomes favorable. Note that the formation of silicene on $MoS_2$ is essentially an endothermic process, but in very Si-rich conditions, the formation of LHD silicene becomes exothermic. This is not surprising and a similar trend has been reported in the phase diagram of both silicene on $SnS_2$ and on Ag(111) [75,76]. Based on the phase diagram of Fig. 6c one can speculate that in Si-poor conditions and at relative high temperature, the formation of LSMS is plausible, while increasing the Si chemical potential, the growth mechanism or phase transformation in LHD silicene is favorable, even at much lower temperature. On the contrary, the surface formation of HB silicene on $MoS_2$ is much higher in energy, as compared to LSMS and LHD silicene, thus it is predicted to be thermodynamically not stable under equilibrium conditions, but it may be stabilized, e.g. by kinetic effects during growth or by (surface) defects-mediated growth mechanisms. This is confirmed by our DFT simulations of a 4x4 $MoS_2$ supercell with HB silicene on top. After ionic relaxation the honeycomb lattice of the initial HB silicene on $MoS_2$ is broken, and a disordered layer is formed even at 0 K. The surface energy of the disordered layer (plotted in Fig. 6c) is much lower than that of HB silicene on $MoS_2$, indicating that the HB phase is a local minimum of the potential energy surface of silicene on $MoS_2$, only if the symmetry constrain of the 1x1 cell is kept. On the other hand, our MD simulations show that the large supercells of LSMS and LHD silicene on $MoS_2$ maintain their geometry after 10 ps at 500 K. We want to stress that our simulations do not take into account possible kinetic effects, nor defects on the surface of the layered $MoS_2$, thus they can not rule out HB silicene as a possible phase observed in experiments. However, if the growth of HB silicene on $MoS_2$ will be confirmed by further experimental and theoretical studies, this would be also a confirmation that the growth of LSMS and LHD silicene at lower temperature is also possible.

Silicene can also be potentially synthesized on other transition metal dichalcogenides, having lattice parameters closer to the LB free-standing silicene one, and leading to much reduced in-plane compressive strain in the silicene layer. Such templates are e.g. $MoSe_2$ and $MoTe_2$; bulk $MoSe_2$ and $MoTe_2$ are indirect bandgap materials, with a gap of about 1.1 and 1.0 eV, respectively [55,56]. The unit cell of the hexagonal structure of $MoSe_2$ and $MoTe_2$ has an in-plane lattice parameter of about 3.3 and 3.5 Å,

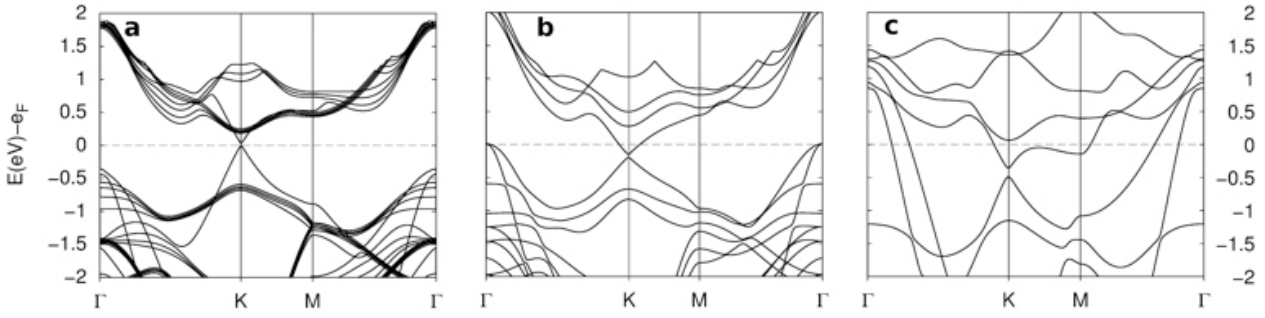


**Figure 8** Electronic band structure of the silicene layer on bulk $MoTe_2$(a), monolayer $MoTe_2$(b) and $MoSe_2$(c). Reproduced with kind permission from IOP Publishing, ref. [35].

respectively, i.e. about 15% and 9% smaller than free standing silicene.

In ref [35] different initial atomic configurations of the Si atoms were considered on $MoSe_2$ or $MoTe_2$, like in the $MoS_2$ case, finding that after energy relaxation, the different configurations show almost the same total energy, typically within 10 meV/atom. For all the studied configurations, the flat silicene layer, both on $MoSe_2$ and $MoTe_2$, buckled after the atomic relaxation, with a buckling distance of about 1 Å on $MoSe_2$ and 0.7 Å on $MoTe_2$; this latter value is very close to the buckling estimated for the 3x3 silicene layer on Ag (111) [6]. Very interestingly, its calculated electronic band structure (see Fig. 8.a) revealed that silicene on bulk $MoTe_2$ is a gapless-semiconductor, due to the typical mixed $sp^2/sp^3$-like hybridization of the Si atoms in low buckled silicene [57]. On the other hand, the calculations of silicene on a monolayer $MoTe_2$ or placed in between two $MoTe_2$ layers revealed that silicene presents a higher buckling (~0.77 Å), as compared to the case of bulk $MoTe_2$ substrate, due to the stronger interaction of the silicene layer with the $MoTe_2$ monolayer. This was confirmed by the adhesion energy of silicene in the two systems, which is about 5% higher for silicene on monolayer $MoTe_2$ than silicene on bulk $MoTe_2$. Consequently, silicene on a $MoTe_2$ monolayer or in between two $MoTe_2$ layers was predicted to be metallic, as shown in Fig. 8.b, though with preserved Dirac cones at the K points. Similarly, the study of silicene on bulk $MoSe_2$ as well as on $MoSe_2$ monolayer or in-between two $MoSe_2$ layers revealed that these systems are metallic (see Fig. 8.c), due to the substantial higher buckling of silicene on $MoSe_2$ with respect to silicene on $MoTe_2$. From a thermodynamic point of view, the case of silicene on $MoSe_2$ is expected to be very similar to the $MoS_2$ one, showing a meta-stable HB silicene, but also more stable silicene layers with low buckled low strain or dumbbell phases. The case of $MoTe_2$ is slightly different; because of the much reduced strain of the silicene layer on the 1x1 $MoTe_2$, being very close to a LB phase, its surface energy is much lower compared to HB silicene on $MoS_2$ (see Fig. 6c). The 1x1 silicene and LHD phase on $MoTe_2$ are also much closer to each other in the phase diagram of Fig. 6c, when compared to the $MoS_2$ case. Note also that the growth of LHD silicene on $MoTe_2$ is much less favorable than on $MoS_2$. The main reason for this difference between $\sqrt{3}\times\sqrt{3}$ LHD silicene on 4x4 $MoS_2$ and LHD silicene on 1x1 $MoTe_2$ can be still attributed to a marked strain effect on the silicene layer in the latter case.

These theoretical studies suggest that the electronic properties of silicene layers, van der Waals bonded on transition metal dichalcogenides, can be tuned by the appropriate choice of the substrate material and growth conditions; the electronic structure of silicene is indeed predicted to be correlated to the buckling of the Si atoms, which in turns depends on the interactions between the silicene layer and the substrate.

Further experimental progress has been achieved very recently, pertaining to the successful fabrication of back-gated field effect transistors based on a 2D silicon layer on $MoS_2$ [58]. The $MoS_2$ layers were first mechanically exfoliated on $SiO_2$/p++Si substrates. Au/Ti source/drain contacts were deposited on the $MoS_2$ flakes and patterned using electron beam lithography. Si nanosheets were subsequently grown on $MoS_2$ at 200 °C in a MBE

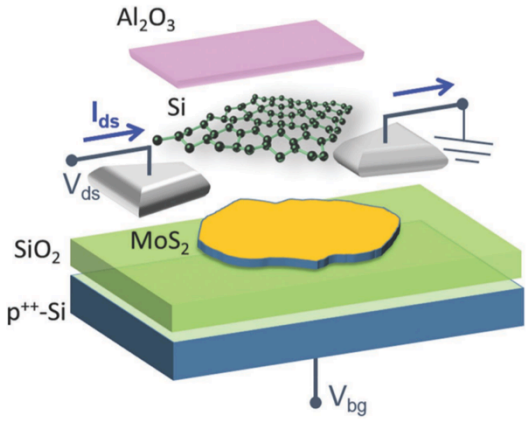


**Figure 9** Sketch of the back-gated $MoS_2$/silicene/$Al_2O_3$ field effect transistor. Reproduced with kind permission from Wiley Publishing, ref. [58].

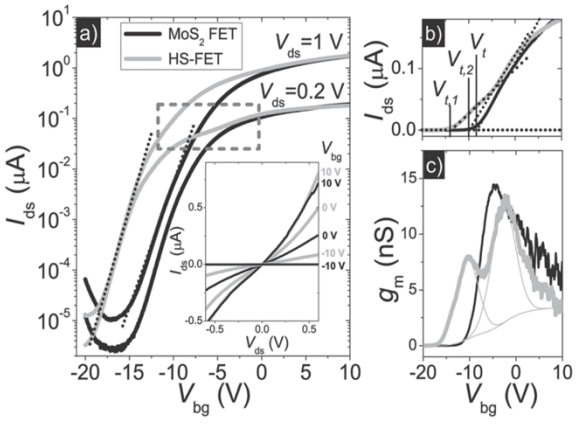


**Figure 10** Semi-logarithmic plot of the transfer curves of $MoS_2$ (black lines) and $MoS_2$/silicene (grey lines) field effect transistors at 0.2 and 1 V source-drain voltage ($V_{ds}$). The region with an extra field modulation of the silicene/$MoS_2$ device is framed with a dashed line. Inset: corresponding output characteristics as a function of the bottom gate bias ($V_{bg}$). b) plot of the transfer characteristics, emphasizing the double threshold in the silicene/$MoS_2$ devices. c) Transconductance $g_m$ as a function of gate bias of the $MoS_2$ (black lines) and $MoS_2$/silicene (grey lines) devices, obtained at $V_{ds}$=0.2 V. Reproduced with kind permission from Wiley Publishing, ref. [58].

reactor. The silicene sheets were next capped with 5 nm thick $Al_2O_3$ layers, grown by reactive molecular beam deposition. A schematic sketch of the device is shown in Fig. 9.

The drain current-gate voltage characteristics of these devices are shown in Fig. 10 (a) and (b). The transfer characteristic of a reference device (without the silicene layer on $MoS_2$) is also shown for comparison. Very good $I_{on}/I_{off}$ ratios are reported (about $10^4$ to $10^5$), demonstrating the electrostatic control of the channel. There is a noticeable difference between the $MoS_2$ and Si/$MoS_2$ interface based devices, highlighted in Fig. 10(c), where the transconductance $g_m$ is presented as a function of the gate bias. Two peaks in $g_m$ are clearly observed in the Si/$MoS_2$ heterosheet interface, likely indicating that two conducting channels are formed in these devices: a channel at the $MoS_2$/$SiO_2$ interface, and an additional one formed at the Si/$MoS_2$ interface, due to the accumulation of electrons at this interface. Further evidence of this charge transfer process at the Si/$MoS_2$ interface was obtained from angle-resolved photoemission spectroscopy and scanning tunneling spectroscopy measurements [58].

## 3. Silicene/substrate interaction: covalent bonding

The formation of covalent bonds between silicene and an underlying substrate can result in the partial or complete $sp^3$ hybridization of the Si atoms, and consequently, in the opening of an energy gap in its electronic structure – like e.g. in silicene functionalized by the adsorption of ad-atoms [59-64]; we discuss here the covalent bonding between silicene and ZnS surfaces [65,66], as a typical example of a stronger interaction (compared to the weak van der Waals bonding) between silicene and a non-metallic substrate.

ZnS crystallizes in the Wurtzite phase [67,68] and is a semiconductor, with a direct energy band-gap of about 3.8 eV. Interestingly, its in-plane lattice constant (3.81 Å) is very close to the computed one of free-standing silicene, (about 3.9 Å), ZnS thus appearing as an ideal non-metallic template for the growth of silicene. A (0001) polar ZnS surface was considered in ref. [65] as a possible template for silicene. Displacements of the top and bottom ZnS layers was observed during atomic relaxation, resulting in a surface reconstruction very similar to the one of the non-polar (1010) ZnS surface [69,70], as

discussed in more details in refs. [65,71]. The reconstructed (0001) ZnS surface was found to be semiconducting, with a computed energy gap of about 2.5 eV, and was predicted to be more stable than the non-reconstructed polar surface for layers up to about 6.6 nm [71]. Note that the polar (non-reconstructed) ZnS surface is metallic, due to the pining of the Fermi level by the anion surface states, like in ZnO [72,73]. On such a polar surface, silicene was also predicted to be metallic [74].

To study the interaction of silicene with the reconstructed (0001) ZnS surface, a slab with a flat silicene layer on top of the surface was modeled, followed by atomic relaxation. Different possible arrangements of the Si atoms on the (0001) ZnS surface were considered, as discussed in more details in ref. 65. The most energetically stable structure is reproduced in Fig. 11, and corresponds to a hexagonal arrangements of the Si atoms placed at intermediate positions between top and hollow sites of the ZnS hexagons. Two Si-S bonds and two Si-Zn bonds are formed, with a charge transfer essentially involving the $3p_z$ orbitals of the Si atoms and the 4s states of Zn and 3p states of S, the bonded Si atoms thus adopting an $sp^3$-like character. Four other Si

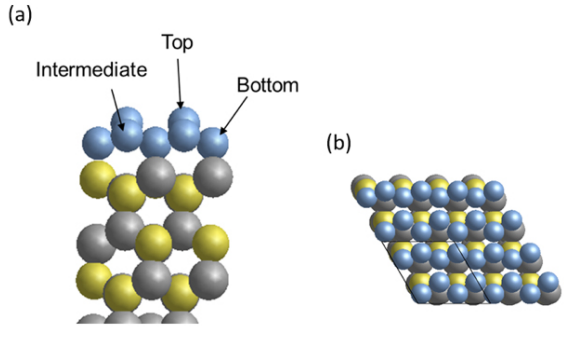


**Figure 11** Side view (a) and top view (b) of the relaxed silicene/(0001) ZnS slab model. Yellow, gray and blue spheres are S, Zn and Si atoms, respectively. Reproduced with kind permission from RSC Publishing, ref. [65].

atoms are not bonded to the ZnS surface, two of these atoms lying at about 2.64 Å from the surface (marked "intermediate" on Fig. 11) and two other

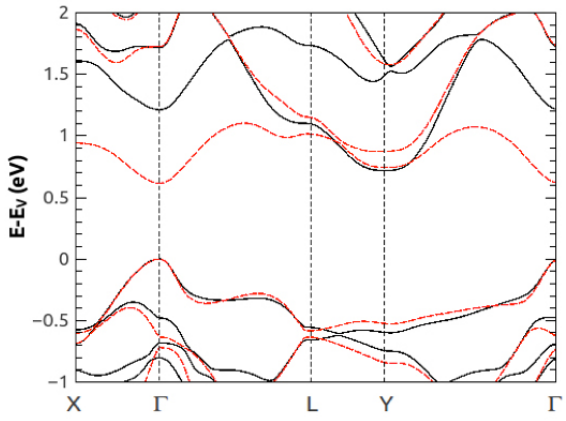


**Figure 12** Computed energy band structure of the silicene/(0001) ZnS slab model, without (solid black lines) and with (dashed red lines) an external electric field of 0.6 V/Å in the direction perpendicular to the interface. The reference (zero) energy level corresponds to the top of the valence band $E_V$ of silicene. Reproduced with kind permission from RSC Publishing, ref. [65].

atoms are lying at about 3.33 Å from the surface (marked "top" on Fig. 11). The charge transfer at the silicene/(0001) ZnS interface leads to an excess of negative (Mulliken) charge of about 0.18 |e| on the top Si atoms, with respect to the intermediate Si atoms, resulting in the formation of a dipole at this interface. The average Si-Si distance (2.30 Å) is very similar to the one of free-standing silicene.

The silicene/(0001)ZnS interface was predicted to be semiconducting, with a computed indirect energy band gap of about 0.7 eV, as shown in Fig. 12. The energy gap opening in silicene is due to the charge transfer and $sp^3$ hybridization of the Si atoms bonded to the Zn or S atoms on the surface. The effect of an out-of-plane electric field on the energy band structure of the system is also illustrated in Fig. 12 (dashed lines). The electric field has a substantial effect on the conduction band near the Γ point, leading to a transition from an indirect (Γ to Y point) to direct (at Γ point) energy band gap in silicene, for an electric field of about 0.5 V/ Å, as indicated in Fig. 13. The electric-field dependence of the energy band gap of the silicene layer is related to the modulation of the electric dipole at the silicene/ZnS interface [65]. Note that an electric field of 0.5 V/ Å appears to be very large. But considering the thickness of the

silicene layer, which corresponds to its buckling distance (typically 0.7 Å on ZnS), it corresponds to a moderate voltage drop of about 0.3 V over the silicene layer.

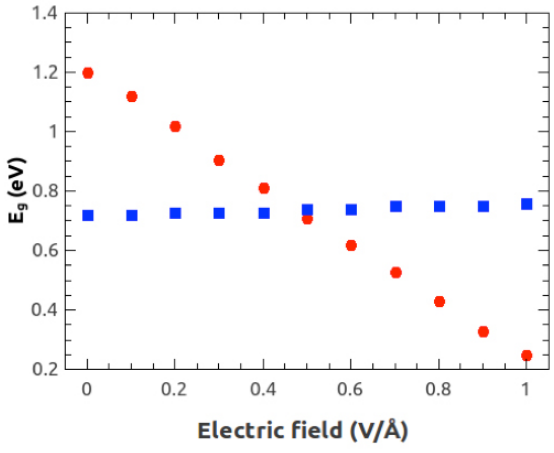


**Figure 13** Computed direct (filled circles) and indirect (filled squares) energy band gaps of the silicene/(0001) ZnS slab model, as a function of the external electric field applied to the system. Reproduced with kind permission from RSC Publishing, ref. [65].

A similar effect of an external electric field applied to a LHD silicene/$SnS_2$ heterostucture was shown recently [75]. In this case, although the interaction between the silicene layer and the substrate is weak, the electric field modifies the charge distribution at the silicene/substrate interface, varying the electronic states of the silicene layer and hence its bandgap. Both cases highlight the non-negligible effect of the substrate on the properties of the silicene layers.

## Summary

The recent progress reported on the growth and characterization of silicene on different substrates is very encouraging. However, so far, only direct experimental evidence of silicene on metallic surfaces has been presented. Its possible integration in future nanoelectronic devices will require its growth on non-metallic substrates. In this manuscript, we have reviewed recent theoretical and experimental works on the possible growth of silicene on non-metallic surfaces.

The weak van der Waals interaction between silicene and e.g. transition metal dichalcogenides can potentially preserve the electronic properties of free-standing silicene, which is predicted to be a gapless semiconductor, like graphene. However, the electronic properties of silicene depend on its buckling, e.g. highly buckled silicene on $MoS_2$ is predicted to be metallic, while low buckled silicene on $MoS_2$ or $MoTe_2$ is predicted to be a gapless semiconductor, with preserved Dirac cones.

On the other hand, the covalent bonding of silicene on e.g. ZnS surfaces leads to the opening of an energy gap in its electronic structure. Very interestingly, the magnitude and nature (direct or indirect) of this energy gap can be controlled by an out-of-plane electric field. Even in the weak interacting silicene/layered chalcogenide hetero -structures, an external electric field can be used to perturb the distribution of the charge at the silicene/substrate interface, modulating its electronic gap. These theoretical predictions are potentially very interesting for silicene-based logic devices.

We have also discussed a new approach to systematically study the stability of silicene in van der Waals hetero- structures, by exploiting the thermodynamic phase diagrams, which can help to link the theoretical predictions and the experimental growth of silicene. The importance of finite-temperature simulations has been emphasized, including larger supercell than the silicene unit cell, for exhaustive theoretical investigations. These methods have been used to study the possible growth of new silicene phases, such as the honeycomb dumbbell silicene, on layered substrates, providing useful indications for the experimental growth conditions.

From an experimental point of view, very encouraging results have been reported on the possible growth of silicene on $MoS_2$. These results could pave the way to silicene-based van der Waals heterostructures for high performances and low-power nanoelectronic devices. Towards this goal, functional silicene/$MoS_2$ field effect transistors have been recently fabricated. Further progress in the material deposition and device integration is required, like the growth of silicene over large areas,

improvement in the quality of the silicene layers to achieve higher carrier mobility, as well as the fabrication of top-gated field-effect transistors.

## Methods

The simulations presented here were performed within ab initio density functional theory (DFT) as implemented in the QUANTUM ESPRESSO Package [77]. The generalized gradient approximation (GGA) as proposed by Perdew, Burke and Ernzerhof was used for the exchange-correlation functional [78]. In addition, the long-range van der Waals interactions between the layers were taken into account in the calculations, by including the DFT-D2 van der Waals correction [79]. The plane wave cut-off energy was set to 500 eV and the energy criterion for the self-consistency iteration to $10^{-5}$ eV. Residual forces during structural relaxation were converged to less than 0.01eV/Å. The bulk $ME_2$ substrates were modeled by using 4 $ME_2$ layers, with the two bottom layers "frozen" at their bulk position. A supercell with more than 15 Å vacuum layer was used for the DFT simulations.

The GGA-DFT bandgap underestimation is a well known issue. The reported gap and particularly the variation of the energy gap with applied electric field shown in Fig. 13 may be affected by this underestimation. When compared to hybrid DFT calculations (i.e. Heyd-Scuseria-Ernzerhof –HSE-), the GGA underestimation of the gap opening in silicene can be well beyond 100%, as recently shown for the case of LHD silicene on $SnS_2$[75]. Although this affects the quantitative estimations of the electronic properties, GGA is expected to still catch trends and the general electronic behaviors, as also confirmed in ref. [75}.

Details about methods used in the revisited works can be found in the respective refs. [30, 35, 54, 65].

## Acknowledgements

This work has been financially supported by the European Project 2D-NANOLATTICES, within the Future and Emerging Technologies (FET) program of the European Commission, under the FET-grant number 270749, as well as the KU Leuven Research Funds, project GOA/13/011. We are grateful to A. Molle (MDM Laboratory), A. Dimoulas (NCSR Demokritos) and G. Pourtois (imec) for their valuable contributions to this work and for stimulating discussions.

## References

[1] K.S. Novoselov, A.K. Geim, S.V. Morozov, D. Jiang, Y. Zhang, S.V. Dubonos, I.V. Grigorieva, and A.A. Firsov, Science 306, 666 (2004).

[2] K.S. Novoselov, D. Jiang, F. Schedin, T. Booth, V.V. Khotkevich, S.V. Morozov, and A.K. Geim, Proc. Natl. Acad. Sci. USA 102, 10451 (2005).

[3] S.Z. Butler et al., ACS Nano 7, 2898 (2013).

[4] G. Fiori, F. Bonaccorso, G. Iannaccone, T. Palacios, D. Neumaier, A. Seabaugh, S.K. Banerjee, and L. Colombo, Nature Nanotechnol. 9, 768 (2014).

[5] F. Schwierz, J. Pezoldt, and R. Granzner, Nanoscale 7, 8261 (2015).

[6] P. Vogt, P. De Padova, C. Quaresima, J. Avila, E. Frantzeskakis, M.C. Asensio, A. Resta, B. Ealet, and G. Le Lay, Phys. Rev. Lett. 108, 155501 (2012).

[7] M.E. Davila, L. Xian, S. Cahangirov, A. Rubio, and G. Le Lay, New J. Phys. 16, 095002 (2014).

[8] M. Derivaz, D. Dentel, R. Stephan, M.C. Hanf, A. Mehdaoui, P. Sonnet, and C. Pirri, Nano Lett. 15, 2510 (2015).

[9] F.F. Zhu, W.J. Chen, Y. Xu, C.L. Gao, D.D. Guan, C.H. Liu, D. Qian, S.C. Zhang, and J.F. Jia, Nature Mater. 14, 1020 (2015).

[10] K. Takeda and K. Shiraishi, Phys. Rev. B 50, 14916 (1994).

[11] S. S. Cahangirov, M. Topsakal, E. Akturk, H. Sahin, and S. Ciraci, Phys. Rev. Lett 102, 236804 (2009).

[12] M. Ezawa, Phys. Rev. Lett. 109, 055502 (2012).

[13] M. Ezawa, New J. Phys. 14, 033003 (2012).

[14] E. Scalise, M. Houssa, G. Pourtois, B. van den Broek, V.V. Afanas'ev, and A. Stesmans, Nano Res. 6, 19 (2013).

[15] L. Matthes, O. Pulci, and F. Bechstedt, New J. Phys. 16, 105007 (2014).

[16] M. Houssa, A. Dimoulas, and A. Molle, J. Phys: Condens. Matter 27, 253002 (2015).

[17] B. Feng, Z. Ding, S. Meng, Y. Yao, X. He, P. Cheng, L. Chen, and K. Wu, Nano Lett. 12, 3507 (2012).

[18] D. Chiappe, C. Grazianetti, G. Tallarida, M. Fanciulli, and A. Molle, Adv. Mat. 24, 5088 (2012).

[19] H. Enriquez, S. Vizzini, A. Kara, B. Lalmi and H. Oughaddou, J. Phys: Condens. Matter 24, 314211 (2012).

[20] D. Tsoutsou, E. Xenogiannopoulou, E. Golias , P. Tsipas, A. Dimoulas, Appl. Phys. Lett. 103, 231604 (2013).

[21] P. Moras, T. O. Mentes, P. M. Sheverdyaeva, A. Locatelli and C. Carbone, J. Phys.: Condens. Matter 26, 185001 (2014).

[22] A. Fleurence, R. Friedlein, T. Ozaki, H. Kawai, Y. Wang, Y. Takamura, Phys. Rev. Lett. 108, 245501 (2012).

[23] C.C. Lee, A. Fleurence, Y. Yamada-Takamura, T. Ozaki, and R. Friedlein, Phys. Rev. B 90, 075422 (2014).

[24] L. Meng, Y. Wang, L. Zhang, S. Du, R. Wu, L. Li, Y. Zhang, G. Li, H. Zhou, W.A. Hofer, and M.J. Gao, Nano Lett. 13, 685 (2013).

[25] L. Tao, E. Cinquanta, D. Chiappe, C. Grazianetti, M. Fanciulli, M. Dubey, A. Molle, D. Akinwande, Nature Nanotech. 10, 227 (2015).

[26] D. Jose and A. Datta, Accounts of Chemical Research 47, 593 (2014).

[27] S. Balendhran, S. Walia, H. Nili, S. Sriram, and M. Bhaskaran, Small 11, 640 (2015).

[28] L.C. Lew Yan Voon, J. Zhu, and U. Schwingenschlögl, Appl. Phys. Rev. 3, 040802 (2016).

[29] A. Molle, J. Goldberger, M. Houssa, Y. Xu, S.C. Zhang, and D. Akinwande, to appear in Nature Mater. (2016).

[30] M. Houssa, G. Pourtois, V.V. Afanas'ev, and A. Stesmans, Appl. Phys. Lett. 97, 112106 (2010).

[31] M. Houssa, G. Pourtois, M.M. Heyns, V.V. Afanas'ev, and A. Stesmans, J. Electrochem. Soc. 158, H107, (2011).

[32] Y. Ding and Y. Wang, Appl. Phys. Lett. 103, 043114 (2013).

[33] J. Zhu and U. Schwingenschlögl, J. Mater. Chem. C 3, 3946 (2015).

[34] D. Chiappe, E. Scalise, E. Cinquanta, C. Grazianetti, B. van den Broek, M. Fanciulli, M. Houssa and A. Molle, Adv. Mater. 26, 2096 (2014).

[35] E. Scalise, M. Houssa, E. Cinquanta, C. Grazianetti, B. van den Broek, G. Pourtois, A. Stesmans, M. Fanciulli, and A. Molle, 2D Mater. 1, 011010 (2014).

[36] J.J. Zhu and U. Schwingenschlögl, ACS Appl. Mat. Interf. 6, 11675 (2014).

[37] L. Linyang, W. Xiaopeng, Z. Xiaoyang, and Z. Mingwen, Phys. Lett. A 377, 2628 (2013).

[38] S. Kokott, P. Pflugradt, L. Matthes, and F. Bechstedt, J. Phys.: Condens. Matter 26, 185002 (2014).

[39] M. Badylevich, S. Shamuilia, V.V. Afanas'ev, A. Stesmans, Y.G. Fedorenko, and C. Zhao, J. Appl. Phys. 104, 093713 (2008).

[40] Y.-N. Xu and W.Y. Ching, Phys. Rev. B 48, 4335 (1993).

[41] C.L. Freeman, F. Claeyssens, N.L. Allan, and J.H. Harding, Phys. Rev. Lett. 96, 066102 (2006).

[42] P. Tsipas, S. Kassavetis, D. Tsoutsou, E. Xenogiannopoulou, E. Golias, S.A. Giamini, C. Grazianetti, D. Chiappe, A. Molle, M. Fanciulli, and A. Dimoulas, Appl. Phys. Lett. 103, 251605 (2013).

[43] K. K. Kam and B. Parkinson, J. Chem. Phys. 86, 463 (1982).

[44] K. F. Mak, C. Lee, J. Hone, J. Shan, and T. F. Heinx, Phys. Rev. Lett. 105, 136805 (2010).

[45] A. Splendiani, L. Sun, Y. Zhang, T. Li, J. Kim, C.Y. Chim, Galli G., and F. Wang, Nano Lett. 10, 1271 (2010).

[46] S. W. Han, H. Kwon, S. K. Kim, S. Ryu, W. S. Yun, D. H. Kim, J. H. Hwang, J.-S. Kang, J. Baik, H. J. Shin, and S. C. Hong, Phys. Rev. B 84, 045409 (2011).

[47] J. N. Coleman, M. Lotya, A. O'Neill, S. D. Bergin, P. J. King, U. Khan, K. Young, A. Gaucher, S. De, R. J. Smith, I. V. Shvets, S. K. Arora, G. Stanton, H.-Y. Kim, K. Lee, G. T. Kim, T. Duesberg, G. S.and Hallam, J. J. Boland, J. J. Wang, J. F. Donegan, J. C. Grunlan, G. Moriarty, A. Shmeliov, R. J. Nicholls, J. M. Perkins, E. M. Grieveson, K. Theuwissen, D. W. McComb, Nellist P. D., and V. Nicolosi, Science 331, 568 (2011).

[48] S. Bertolazzi, J. Brivio, and A. Kis, ACS Nano 5, 9703 (2011).

[49] S. Lebegue and O. Eriksson, Phys. Rev. B 79, 115409 (2009).

[50] T. Li and G. Galli, J. Phys. Chem. C 111, 16192 (2007).

[51] C. Ataca, H. Sahin, E. Akturk, and S. Ciraci, J. Phys. Chem. C 115, 3934 (2011).

[52] D.C. Langreth, M. Dion, H. Rydberg, E. Schroeder, P. Hyldgaard and B.I. Lundqvis, Int. J. Quant. Chem., 101,599-610 (2005).

[53] N. Gao, J.C. Li, and Q. Jiang, Phys. Chem. Chem. Phys. 16, 11673 (2014).

[54] L. Li and M. Zhao, J. Phys. Chem. C 118, 19129 (2014).

[55] J.A. Wilsonand, and .A. D. Yoffe, Adv. Phys. 18, 193-335 (1969).

[56] T. Boker et al., Phys. Rev. B 64, 235305(1)- 235305(11) (2001).

[57] E. Cinquanta et al., J. Phys. Chem. C 117, 16719 (2013).

[58] A. Molle, A. Lamperti, D. Rotta, M. Fianciulli, E. Cinquanta, and C. Grazianetti, Adv. Mater. Interfaces 3, 1500619 (2016).

[59] L.C. Lew Yan Voon, E. Sandberg, R.S. Aga, and A.A. Farajian, Appl. Phys. Lett. 97, 163114 (2010).

[60] M. Houssa, E. Scalise, K. Sankaran, G. Pourtois, V.V. Afanas'ev, and A. Stesmans, Appl. Phys. Lett. 98, 223107 (2011).

[61] R. Quhe, R. Fei, Q. Liu, J. Zheng, H. Li, C. Xu, Z. Ni, Y. Wang, D. Yu, Z. Gao, and J. Lu, Sci. Rep. 2, 853 (2012).

[62] Y. Ding and Y. Wang, Appl. Phys. Lett. 100, 083102 (2012).

[63] B. van den Broek, M. Houssa, E. Scalise, G. Pourtois, V.V. Afanas'ev, and A. Stesmans, Appl. Surf. Sci. 291, 104 (2014).

[64] T.P. Kaloni, N. Singh, and U. Schwingenschlögl, Phys. Rev. B 89, 035409 (2014).

[65] M. Houssa, B. van den Broek, E. Scalise, G. Pourtois, V.V. Afanas'ev, and A. Stesmans, Phys. Chem. Chem. Phys. 15, 3702 (2013).

[66] S.S. Li, C.W. Zhang, S.S. Yan, S.J. Hu, W.X. Ji, P.J. Wang, and P. Li, J. Phys.: Condens. Matter 26, 395003 (2014).

[67] Handbook of Laser Science and Technology, Ed. by M.J. Weber (CRC Press, Cleveland, 1986).

[68] Y.-N. Xu and W.Y. Ching, Phys. Rev. B 48, 4335 (1993).

[69] J. E. Northrup and J. Neugebauer, Phys. Rev. B 53, R10477 (1996).

[70] A. Filippetti, V. Fiorentini, G. Cappellini, and A. Bosin, Phys. Rev. B 59, 8026 (1999).

[71] X. Zhang, H. Zhang, T. He, and M. Zhao, J. Appl. Phys. 108, 064317 (2010).

[72] A. Wander, F. Schedin, P. Steadman, A. Norris, R. McGrath, T.S. Turner, G. Thornton, and N.M. Harrison, Phys. Rev. Lett. 86, 3811 (2001).

[73] B. Meyer and D. Marx, Phys. Rev. B 67, 035403 (2003).

[74] M. Houssa, B. van den Broek, E. Scalise, G. Pourtois, V.V. Afanas'ev, and A. Stesmans, ECS Trans. 53, 51 (2013).

[75] E.Scalise, M. Houssa, Nano Res. 10, 1697 (2017).

[76] P. Pflugradt, L.Matthes, F. Bechstedt. Phys. Rev. B, 89 (2014), 035403.

[77] P. Giannozzi, S. Baroni, N. Bonini, M. Calandra, R. Car, C. Cavazzoni, D. Ceresoli, G. L. Chiarotti, M. Cococcioni, I. Dabo, A. Dal Corso, S. Fabris, G. Fratesi, S. de Gironcoli, R. Gebauer, U. Gerstmann, C. Gougoussis, A. Kokalj, M. Lazzeri, L. Martin-Samos, N. Marzari, F. Mauri, R. Mazzarello, S. Paolini, A. Pasquarello, L. Paulatto, C. Sbraccia, S. Scandolo, G. Sclauzero, A. P. Seitsonen, A. Smogunov, P. Umari, R. M. Wentzcovitch. (2009), 395502.

[78] J.P. Perdew, K. Burke and M. Ernzerhof. Phys. Rev. Lett., 77 (1996), 3865.

[79] Grimme, S. J. Comput. Chem., 27 (2006), 1787.